Homology-Modeled Structure of the Yeast Mitochondrial Citrate Transport Protein

D. Eric Walters and Ronald S. Kaplan
Department of Biochemistry and Molecular Biology, Rosalind Franklin University of Medicine and Science, North Chicago, Illinois 60064

ABSTRACT We have used homology modeling to construct a three-dimensional model of the yeast mitochondrial citrate transport protein (CTP), based on the recently published x-ray crystal structure of another mitochondrial transport protein, the ADP/ATP carrier. Superposition of the backbone traces of the homology-modeled CTP onto the crystallographically determined ADP carrier structure indicates that the CTP transmembrane domains are well modeled (i.e., root mean square deviation of 0.94 Å), whereas the loops facing the intermembrane space and the mitochondrial matrix are less certain (i.e., root mean square deviation values of 0.72–2.06 Å). The homology-modeled CTP is consistent with our earlier de novo models of the transporter's transmembrane domains, with respect to residues which face into the transport path. Importantly, the resulting model is consistent with our previous experimental data obtained from measuring reactivity of 34 single cysteine mutants in transmembrane domains 3 and 4 with methanethiosulfonate reagents. The model also points to a likely dimer interface region. In conclusion, our data help to define the substrate translocation pathway in both the modeled CTP structure and the crystallographic ADP carrier structure.

INTRODUCTION

The mitochondrial citrate transport protein (CTP) from higher eukaryotic organisms catalyzes the obligatory exchange of citrate plus a proton for malate across the inner mitochondrial membrane. The citrate produced in the mitochondria is utilized in the cytoplasm for sterol and fatty acid biosynthesis, and as a source of NAD^+. The CTP is a member of the mitochondrial carrier protein family; these are transporters which shuttle a large number of solutes between cytosol and mitochondria.

We have studied the structure and function of the yeast homolog of the higher eukaryotic transporter since after overexpression, the yeast mitochondrial CTP can be functionally reconstituted in liposomes with high specific activity. Thus this transporter presents an ideal opportunity to conduct a comprehensive structure/function analysis. As part of this effort we have studied the CTP by cysteine-scanning mutagenesis (Kaplan et al., 2000a; Ma et al., 2004), site-directed mutagenesis (Xu et al., 2000), and site-directed spin labeling (Kaplan et al., 2000b). Furthermore, we have shown, using nondenaturing size-exclusion chromatography and native gel electrophoresis, that the CTP is a functional dimer (Kotaria et al., 1999).

Recently the three-dimensional structure of the bovine mitochondrial ADP/ATP carrier was solved by x-ray crystallography at a resolution of 2.2 Å (Pebay-Peyroula et al., 2003). The yeast mitochondrial citrate transporter has sufficient homology with this member of the mitochondrial carrier protein family to permit the construction of a homology-based model. Here we describe the development of such a model, and evaluate this model in terms of our experimental data obtained by cysteine scanning mutagenesis combined with chemical modification of the over-expressed, functionally reconstituted single Cys mutants.

METHODS

Homology modeling was carried out using Molecular Operating Environment (MOE), v. 2003.02 (Chemical Computing Group, Montreal, Canada). The template structure was the recently published mitochondrial ADP/ATP carrier (Pebay-Peyroula et al., 2003; Protein Data Bank code 1OKC). We refer to helices, mitochondrial loops, and cytoplasmic loops using the system described in that article, and shown in Fig. 1 *A*.

The sequence of the citrate transporter (TXTP_YEAST, Swiss-Prot accession No. P38152) was initially aligned with that of the ADP/ATP carrier using the Gap program (algorithm of Needleman and Wunsch, 1970) in the GCG Wisconsin Package (Accelrys, San Diego, CA). The sequences aligned with 28.5% identity and 37.0% similarity (using the BLOSUM62 scoring matrix, Henikoff and Henikoff, 1992). This alignment was compared with multiple alignments found in two on-line protein databases. The Pfam database (Bateman et al., 2002) includes these proteins in entry PF00153, Mitochondrial carrier protein family. This entry includes alignments of over 2000 related proteins, but only covers helices H1, H2, H3, H4, h12, and h34. The PROSITE database (Bairoch and Bucher, 1994) includes these proteins in entry PS50920, Solute carrier repeat. This entry includes alignment of ~400 related proteins, and includes all helices. The Gap, Pfam, and PROSITE alignments are very similar in helices H1, h12, and H2, but differ in helices H3, h34, and H4. The Gap and PROSITE alignments differ significantly in H6.

Homology modeling was carried out in MOE. In regions where the alignment is good, the backbone conformation was based on that of the template structure; where there are gaps in the alignment, stochastic algorithms were used to generate possible backbone conformations, and a family of 10 modeled backbone conformations was generated. Side-chain conformations were selected from a conformation library. The final structures were lightly minimized to alleviate any remaining bad steric

Submitted March 1, 2004, and accepted for publication May 11, 2004.

Address reprint requests to: D. Eric Walters, Professor of Biochemistry and Molecular Biology, Rosalind Franklin University of Medicine and Science, 3333 Green Bay Rd., North Chicago, IL 60064. Tel.: 847-578-8613; Fax: 847-578-3240; E-mail: eric.walters@finchcms.edu.

0006-3495/04/08/907/05 $2.00

doi: 10.1529/biophysj.104.042127

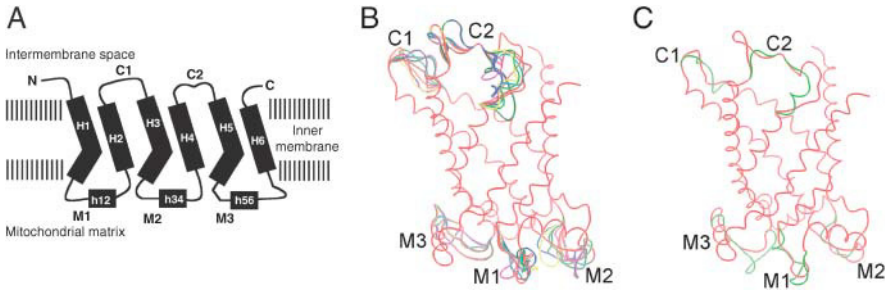

FIGURE 1 (*A*) Schematic representation of the transmembrane helices (H1, H2, H3, H4, H5, and H6), the surface helices (h12, h34, and h56), the intermembrane space loops (C1 and C2), and the mitochondrial matrix loops (M1, M2, and M3). Adapted from Fig. 1 *a* of Pebay-Peyroula et al. (2003). (*B*) Superposition of backbone traces of 10 homology-modeled structures of the citrate transport protein. Each chain is a different color; regions where the backbone trace overlaps appear red. (*C*) Superposition of backbone traces of the best-scoring homology-modeled citrate transporter (*red*) and the crystallographically determined ADP/ATP carrier (*green*). Cytosolic and mitochondrial loop regions are labeled as in *A*.

contacts. The final model was checked using WHAT_CHECK (Hooft et al., 1996), to search for deviations from normal protein conformational parameters. Where necessary, some side-chain conformations were adjusted by selection of alternative conformers from a conformation library.

RESULTS AND DISCUSSION

Model construction and assessment

Comparison of the Gap, Pfam, and PROSITE alignments with the crystal structure of the ADP/ATP carrier enabled us to identify the appropriate alignments in several cases. It is expected that the transmembrane helical segments should be aligned well, and that gaps in the alignment should occur in the mitochondrial and cytoplasmic loops. Further, we expect that, in the transmembrane segments, hydrophobic side chains should generally face the lipid of the membrane, whereas polar side chains should face the transport path. For example, the PROSITE alignment of the two sequences includes a gap in H6. We could identify three possible ways to align the sequences in H6, as shown in Fig. 2. Each of these alignments produces three identical matches as well as some residue similarities. The first of these would place R279 facing into the transport path; the second would appear to place the R279 side chain in the bilayer. The third could place R279 in the transport path, but would require a somewhat strained side-chain conformation. All three alignments were used for construction of homology models. Alignment 1 of Fig. 2 *B* provided the most consistent models; the other two alignments produced disorder in H6.

As illustrated in Fig. 1 *B*, the 10 modeled backbone conformations of the citrate transport protein superimpose extremely well in the transmembrane helical region. Fig. 1 *C* shows that the highest scoring model also superimposes well on the crystal structure of the ADP/ATP carrier which was used as a template in this region. Alpha-carbons of the six transmembrane helices of the highest scoring model superimposed with those of the ADP/ATP carrier with root mean square deviation (RMSD) of 0.94 Å. It can be seen in Fig. 1 *C* that the loops connecting the helices do not superimpose as well, due to lower homology and to insertions and deletions relative to the template sequence. This is reflected in the fact that loops M1, C1, M2, C2, and M3 had RMSDs of 1.03 Å, 2.06 Å, 1.89 Å, 0.72 Å, and 1.98 Å, respectively, when comparing the highest scoring model to the crystal structure. Note that, although the C2 loop has a low RMSD, the RMSD is calculated only on those residues which align; this loop has a substantial insertion in going from the ADP/ATP carrier (seven residues) to the CTP (13 residues). These results are consistent with the expectation that the tertiary structure of the core of the protein is more highly conserved than that of the surface loops.

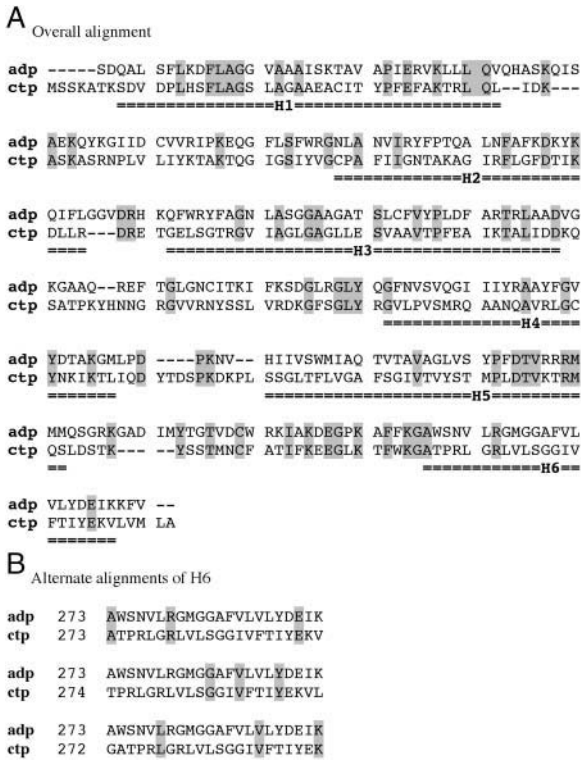

FIGURE 2 (*A*) Alignment of the bovine ADP/ATP carrier and citrate transport protein sequences (labeled ***adp*** and ***ctp***, respectively). Shading indicates alignment of identical residues; *o*verall alignment, with the six major helices indicated. (*B*) Three possible alignments of the residues in helix H6. In each case, the bovine ADP/ATP carrier sequence is listed first, beginning with residue A273.

The final model was evaluated using the WHAT_CHECK program, as described in Methods. This program compares the protein structure to ''normal'' values for proteins available in the Protein Data Bank; thus, the protein is largely being compared to globular proteins rather than membrane proteins. WHAT_CHECK reports errors (features that appear to be incorrect, such as nonplanarity of aromatic rings), warnings (features that are unusual but may be correct, and which should be examined, such as unusual backbone torsion angles), and *notes* (features which were checked and appear to be normal). Bond lengths and bond angles scored within normal limits: the RMS Z-score for bond lengths is 0.46, and the RMS Z-score for bond angles is 1.21. In addition, the Ramachandran Z-score, which measures deviation of backbone torsion angles from commonly seen distributions, was well within the normal range of values. The main exception was the finding that the M3 loop has a number of unusual backbone torsion angles and unsatisfied hydrogen bond donors. This indicates that the M3 loop is not currently well modeled.

We have previously modeled individual transmembrane helices de novo (Walters and Kaplan, 2000) and have proposed ways in which they might pack to form a transport path. We considered arrangements in which the helices are arranged in a *clockwise* manner when viewed from outside the mitochondrial inner membrane, and in which the helices are arranged in a *counterclockwise* manner. The crystal structure demonstrates that the helices are, in fact, arranged counterclockwise. In our previous modeling we predicted that 30 polar and charged residues should face into the transport path (Fig. 4 of Walters and Kaplan, 2000); these are listed in Table 1. Of these, 21 are facing the transport path in our homology-modeled structure. Four are found to be part of loops rather than helices, and one is at the top of a helix. S20 and T81 appear to be positioned in such a way that they can form a pair of hydrogen bonds between the side chains. S231 is facing away from the transport path, but may be able to form side-chain hydrogen bonds to neighboring Y230 or C192. E122 is the only polar/charged residue facing away from the transport path without an apparent partner. We discuss this residue below, as part of the proposed dimer interface.

TABLE 1 Polar and charged residues previously predicted to be part of the transport pathway (Walters and Kaplan, 2000)

Helix	Residue	Position in model
H1	S15	+
	S20	H-bond pair with T81
	E26	+
	T30	+
	E34	+
H2	S68	+
	N80	+
	T81	H-bond pair with S20
	K83	+
	R87	+
H3	E122	Facing outward
	S123	+
	T128	+
H4	R181	+
	Q182	+*
	N185	+
	Q186	+
	R189	+
	Y193	+
H5	S214	Loop
	T217	Loop
	S224	+
	T228	+
	S231	Facing outward
	T232	+
H6	R279	+
	S283	+
	T289	Top of helix
	E292	Loop
	K293	Loop

The third column indicates the location of the side chain in the homology-modeled structure; ''+'' indicates the residue faces the transport path; ''loop'' indicates the residue is not part of the helix; positions of others are noted in the table.

*This side chain can also adopt a conformation in which part of the side chain faces outward; see text for discussion.

Comparison of the CTP homology model with MTS, site directed mutagenesis, and spin labeling experimental data

In earlier studies, we have mutated residues of H3 and H4, one at a time, to cysteine (Kaplan et al., 2000a; Ma et al., 2004). Each mutant was expressed, isolated, and functionally reconstituted in a liposomal system. The accessibility of each single cysteine was assessed by reacting with two different methanethiosulfonate (MTS) reagents.

Our MTS reactivity data for the yeast CTP were mapped onto the transmembrane residues of the homology-modeled structure. The following residues were found to be highly reactive (colored *green*): L116, L120, S123, V127, E131, K134, T135, G174, V178, Q182, N185, and Q186. The following residues were found to have little or no reactivity (colored *magenta*): G117, A118, L121, V124, A125, A126, T128, P129, F130, A132, I133, A136, L137, V175, L176, P177, S179, M180, A183, A184, A187, and V188. A molecular surface was calculated and colored according to residue color; this is shown in Fig. 3 *A*.

Fig. 3 *A* (*left side*) shows the calculated surface as viewed from the side (within the plane of the lipid bilayer). All of the residues facing the lipid phase were relatively unreactive toward MTS reagents, as would be expected. The view in Fig. 3 *A* (*right side*) is from above the bilayer, looking down into the transport path. Residues facing into the pathway were shown experimentally to be highly reactive toward MTS reagents. Thus the modeled structure is consistent with the experimental reactivity data we previously obtained on H3 and H4.

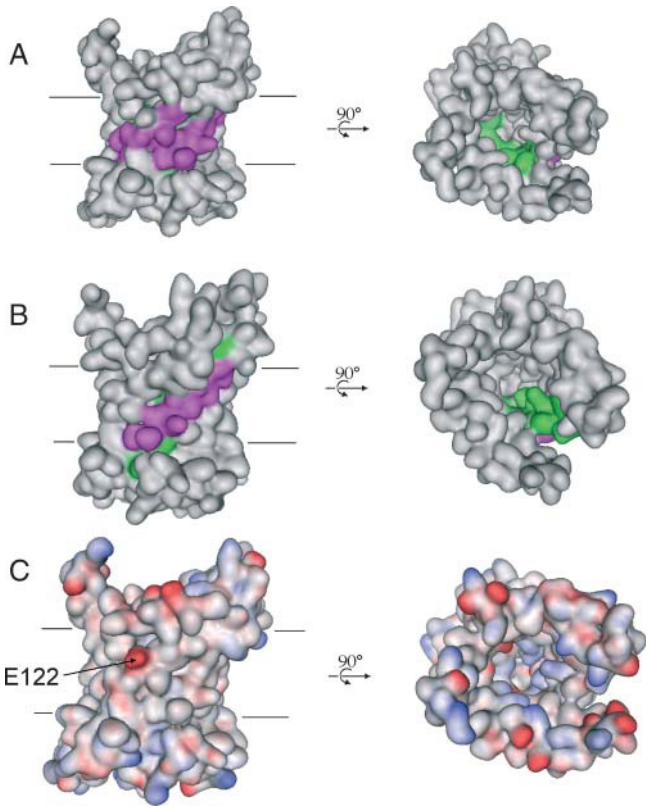

FIGURE 3 (*A*) Molecular surface on homology-modeled yeast CTP, colored according to MTS reactivity as described in the text (*green*, highly reactive; *magenta*, relatively low reactivity). (*Left*) View from the side (in the plane of the membrane) with approximate position of bilayer indicated. (Right) View looking down into the transport pathway (looking down onto the membrane). (*B*) Molecular surface on homology-modeled yeast CTP, colored according to oxygen accessibility data as described in the text (*magenta*, oxygen accessible/facing lipid; *green*, oxygen inaccessible/facing transport path). (*Left*) View from the side (in the plane of the membrane). (*Right*) View looking down into the transport pathway (looking down onto the membrane). (*C*) Molecular surface on homology-modeled yeast CTP, colored according to partial atomic charge as described in the text (*red*, negative charge; *blue*, positive charge). (*Left*) View from the side (in the plane of the membrane). (*Right*) View looking down into the transport pathway (looking down onto the membrane).

Site directed mutagenesis (Xu et al., 2000) showed that R181 and R189 are required for transport function. Our homology-modeled structure places these two residues with side chains facing into the transport path as well.

Single cysteine mutants in H4 were spin labeled, and their oxygen accessibilities were measured using electron paramagnetic resonance (Kaplan et al., 2000b). In this experiment, residues facing the lipid are expected to be oxygen accessible, whereas residues facing the transport path are not. Fig. 3 *B* shows the oxygen accessibility experimental data mapped onto the surface of the homology-modeled CTP. The side view (Fig. 3 *B*, *left side*) shows that residues facing the lipid are, as expected, oxygen accessible (colored *magenta*), whereas the view down into the transport path (Fig. 3 *B*, *right side*) illustrates that the residues facing the transport path are not oxygen accessible (colored *green*). Thus, the model is also consistent with the spin labeling experiments.

Mapping electrostatic potential

If our model is a reasonable one, the surface facing the lipid bilayer should be composed of neutral residues, and the transport path should contain a number of charged and polar residues to facilitate movement of charged solutes. We applied AMBER partial atomic charges to our model (Cornell et al., 1995) and generated a surface colored on the basis of partial atomic charge, shown in Fig. 3 *C*. All of the surface facing the lipid is neutral with the exception of E122, as shown in Fig. 3 *C* (*left side*). This residue was discussed above, and will receive further attention in the following section. Fig. 3 *C* (*right side*) illustrates the view looking into the transport path. Numerous charged and polar residues line this path, including E26, E34, K83, R87, K95, E131, K134, R181, Q182, N185, R189, K208, D236, Q237, R276, and R279.

Proposed dimer interface

The glutamate residue E122 is part of H3. Previous modeling (Walters and Kaplan, 2000) demonstrated that the three polar/charged residues of H3 (E122, S123, and T128) cannot all be on one face of a standard α-helix; we proposed that this helix may form part of the interface of the functional dimer, with one or more of these polar residues participating in the dimer interface. We also proposed that two highly conserved glycines on this helix (G115 and G119) can form part of the dimer interface; their lack of side chains may allow close packing of two H3s. The G115C and G119C single mutations led to 88% and 100% loss of transport activity, respectively (Ma et al., 2004).

In our homology model, these two glycines are facing outward, which would permit such an interface to occur. If two copies of the homology-modeled monomer are placed in such a way as to pack these glycines together, E122 of one monomer is placed in close proximity to the H3-H4 interface of the other monomer, as illustrated schematically in Fig. 4.

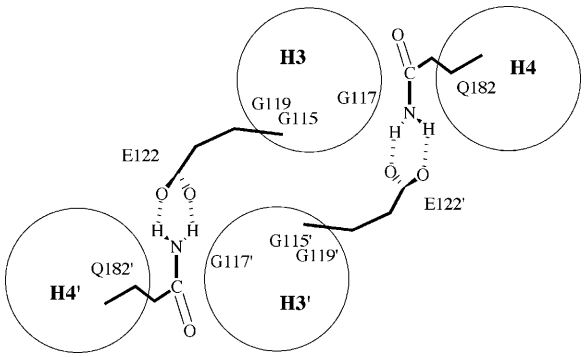

FIGURE 4 Schematic representation of a proposed dimer interface involving E122 of H3 and Q182′ of H4′.

It is most interesting to note that, in the vicinity of the carboxylate group of E122, there is the side chain amide of Q182′ (where Q182′ indicates Q182 of the other monomer). In the homology-modeled structure, Q182 occupies a position at the interface of H3 and H4, such that its side chain can adopt stable conformations facing into the transport path and away from it. In fact, a third glycine in this area, G117′, lacking a side chain, permits Q182′ to adopt a stable conformation in which the side chain carbonyl oxygen points into the transport path, and the side-chain NH_2 group points out toward the lipid. This would position the NH_2 group of Q182′ so that it could hydrogen bond with the carboxylate of E122. The E122-Q182′ and E122′-Q182 interactions could couple the conformational changes of the two transport paths, causing the system to function as an antiporter. Consistent with this view is our finding that mutation of E122 to cysteine resulted in severe loss of function (Ma et al., 2004).

Could this type of interaction occur in the ADP/ATP carrier? According to our alignment, E122 of the CTP corresponds to T125 of the ADP/ATP carrier, and this residue faces away from the transport path in the crystal structure. Q182 of the CTP corresponds to R187 of the ADP/ATP carrier. Q182 faces into the transport path in the crystal structure, but could also adopt side-chain conformations in which the guanidinium group faces outward. The three glycines on H3 of the CTP (G115, G117, and G119) correspond to S118, G120, and A122 of the ADP/ATP carrier; these small side chains are oriented in a way which would permit close packing, just as we propose for the CTP.

In summary, the development of a high-quality homology model of the CTP, in combination with substantial functional data, provide important insight into the location of the functionally identified transport pathway within the three-dimensional structure. The use of thiol cross-linking, electron paramagnetic resonance, and novel crystallization strategies to obtain distances and crossing angles between packed helices in the CTP tertiary structure, together with ongoing functional studies, should in the near future provide the additional detail necessary to develop a comprehensive understanding of the CTP mechanism, including the location of its substrate binding site and the complete translocation pathway.

REFERENCES

Bairoch, A., and P. Bucher. 1994. PROSITE: recent developments. *Nucleic Acids Res.* 22:3583–3589. http://us.expasy.org/prosite/.

Bateman, A., E. Birney, L. Cerruti, R. Durbin, L. Etwiller, S. R. Eddy, S. Griffiths-Jones, K. L. Howe, M. Marshall, and E. L. L. Sonnhammer. 2002. The Pfam protein families database. *Nucleic Acids Res.* 30:276–280. http://www.sanger.ac.uk/Software/Pfam/.

Cornell, W. D., P. Cieplak, C. I. Bayly, I. R. Gould, K. M. Merz, Jr., D. M. Ferguson, D. C. Spellmeyer, T. Fox, J. W. Caldwell, and P. A. Kollman. 1995. A second generation force field for the simulation of proteins and nucleic acids. *J. Am. Chem. Soc.* 177:5179–5197.

Henikoff, S., and J. G. Henikoff. 1992. Amino acid substitution matrices from protein blocks. *Proc. Natl. Acad. Sci. USA.* 89:10915–10919.

Hooft, R. W. W., G. Vriend, C. Sander, and E. E. Abola. 1996. Errors in protein structures. *Nature.* 381:272.

Kaplan, R. S., J. A. Mayor, D. Brauer, R. Kotaria, D. E. Walters, and A. M. Dean. 2000a. The yeast mitochondrial citrate transport protein. Probing the secondary structure of transmembrane domain IV and identification of residues that likely comprise a portion of the citrate translocation pathway. . *J. Biol. Chem.* 275:12009–12016.

Kaplan, R. S., J. A. Mayor, R. Kotaria, D. E. Walters, and H. S. Mchaourab. 2000b. The yeast mitochondrial citrate transport protein: determination of secondary structure and solvent accessibility of transmembrane domain IV using site-directed spin labeling. *Biochemistry.* 39:9157–9163.

Kotaria, R., J. A. Mayor, D. E. Walters, and R. S. Kaplan. 1999. Oligomeric state of wild-type and cysteine-less yeast mitochondrial citrate transport proteins. *J. Bioenerg. Biomembr.* 31:543–549.

Ma, C., R. Kotaria, J. A. Mayor, L. R. Eriks, A. M. Dean, D. E. Walters, and R. S. Kaplan. 2004. The mitochondrial citrate transport protein. Probing the secondary structure of transmembrane domain III, identification of residues that likely comprise a portion of the citrate transport pathway, and development of a model for the putative TMDIII-TMDIII' interface. *J. Biol. Chem.* 279:1533–1540.

Needleman, S. B., and C. D. Wunsch. 1970. A general method applicable to the search for similarities in the amino acid sequence of two proteins. *J. Mol. Biol.* 48:443–453.

Pebay-Peyroula, E., C. Dahout-Gonzalez, R. Kahn, V. Trezeguet, G. J.-M. Lauquin, and G. Brandolin. 2003. Structure of mitochondrial ADP/ATP carrier in complex with carboxyatractyloside. *Nature.* 426:39–44.

Walters, D. E., and R. S. Kaplan. 2000. Models of the transmembrane domains of the yeast mitochondrial citrate transport protein. *J. Mol. Model.* 6:587–594.

Xu, Y., D. A. Kakhniashvili, D. A. Gremse, D. O. Wood, J. A. Mayor, D. E. Walters, and R. S. Kaplan. 2000. The yeast mitochondrial citrate transport protein. Probing the roles of cysteines, Arg181, and Arg189 in transporter function. *J. Biol. Chem.* 275:7117–7124.